ACTUATORS

Electrospun liquid crystal elastomer microfiber actuator

Qiguang He[1], Zhijian Wang[1], Yang Wang[2], Zijun Wang[2], Chenghai Li[1], Raja Annapooranan[2], Jian Zeng[1], Renkun Chen[1,2], Shengqiang Cai[1,2]*

Fibers capable of generating axial contraction are commonly seen in nature and engineering applications. Despite the broad applications of fiber actuators, it is still very challenging to fabricate fiber actuators with combined large actuation strain, fast response speed, and high power density. Here, we report the fabrication of a liquid crystal elastomer (LCE) microfiber actuators using a facile electrospinning technique. Owing to the extremely small size of the LCE microfibers, they can generate large actuation strain (~60 percent) with a fast response speed (<0.2 second) and a high power density (400 watts per kilogram), resulting from the nematic-isotropic phase transition of liquid crystal mesogens. Moreover, no performance degradation is detected in the LCE microfibers after 10^6 cycles of loading and unloading with the maximum strain of 20 percent at high temperature (90 degree Celsius). The small diameter of the LCE microfiber also results in a self-oscillatory behavior in a steady temperature field. In addition, with a polydopamine coating layer, the actuation of the electrospun LCE microfiber can be precisely and remotely controlled by a near-infrared laser through photothermal effect. Using the electrospun LCE microfiber actuator, we have successfully constructed a microtweezer, a microrobot, and a light-powered microfluidic pump.

INTRODUCTION

Microfibers can be found in nature and have been extensively explored for a variety of engineering applications. Fibers composed of functional materials have been recently developed as sensors to capture various signals (*1*–*3*). Fiber actuators, powered by different stimuli, have been explored to build assistive devices and structures (*4*–*6*). Versatile actuation modes of animal muscles also originate from the axial contraction of muscle fibers with diameter ranging from 10 to 100 μm (*7*, *8*). Although fiber actuators have been extensively explored for robotics applications, microfiber actuators with comparable performance as animal muscle fibers are not yet available (*9*, *10*).

Liquid crystal elastomer (LCE) has recently shown to be a promising soft actuating material (*11*, *12*). LCE-based soft actuators can generate giant and reversible actuation strain (~50%) caused by the nematic-isotropic phase transition, which have been intensively explored in soft robotics and active morphing structures (*13*–*19*). LCE fiber actuators have also been previously fabricated. For instance, Roach *et al.* (*20*) used a three-dimensional (3D) printing technique to make long LCE fibers for the applications of smart textiles; Naciri *et al.* (*21*) prepared LCE fibers through melt drawing and demonstrated that the LCE fibers can be used as an artificial muscle. Pang *et al.* (*22*) synthesized light-responsive LCE fibers exhibiting a contraction strain around 80%. However, the diameters of those previously studied LCE fibers are often large (>0.3 mm), leading to their slow thermo-actuation speed compared with animal muscle.

Electrospinning technique has been extensively explored for the mass production of continuous fibers with small diameters (*23*, *24*). In the electrospinning process, with an applied high voltage between the polymer solution and a conductive target, the solvent evaporates and dry polymer fibers form, and the electrospun polymer fibers can be collected from the target. Electrospun fibers have been explored for composite reinforcement (*25*, *26*), air filtration (*27*, *28*), scaffolds for tissue regeneration (*29*), and smart textiles (*30*). The diameter, morphology, and properties of electrospun polymer fibers depend on the electrospinning parameters, such as the voltage, polymer concentration, environmental temperature, and humidity (*31*).

Here, we develop a facile method to fabricate thin LCE microfibers through an electrospinning technique. The electrospun LCE microfibers have the diameter around 10 to 100 μm and can generate large actuation strains (greater than 50%) within a fraction of a second, powered by either environmental heating or near-infrared (NIR) laser irradiation. The actuation stress, strain, and power density of the LCE microfibers are all comparable to the performance of human muscle fiber. Using the LCE microfibers, we further build an electrically controlled microtweezer, a microrobot, and a light-powered microfluidic pump.

RESULTS

Fabrication of electrospun LCE microfibers

In the experiment, we used RM 257 as a liquid crystal mesogen and hexane dithiol (HDT) as a chain extender (fig. S1). We prepared electrospinning ink by dissolving the synthesized oligomers into chloroform. Detailed ink preparation can be found in the Supplementary Materials. As shown in Fig. 1A (left), during the electrospinning process, the ink was injected at a constant flow rate (0.02 ml/min) by a syringe pump. We used a metallic mesh to collect the electrospun LCE microfibers. We connected the syringe needle to the positive electrode of a high-voltage (6 kV) power supply and the metallic mesh to the negative electrode. During the electrospinning process, we exposed the LCE microfibers to ultraviolet (UV) light (365-nm wavelength) to trigger the cross-linking reaction. Figure 1A (middle) shows the electrospun LCE microfibers on the metallic mesh collector. The as-spun LCE microfibers were suspended on the collector so they could be easily picked up. The diameters of the electrospun LCE microfibers ranged from 10 to 100 μm, which is comparable to the diameters of human muscle fiber (Fig. 1A, right, and fig. S2).

These as-spun LCE microfibers are in polydomain state (Fig. 1B), as confirmed by the polarized optical microscopic (POM) images (Fig. 1B, bottom). For a polydomain LCE, the nematic domains are randomly distributed. There was no brightness difference of the

---

[1]Department of Mechanical and Aerospace Engineering, University of California, San Diego, La Jolla, CA 92093, USA. [2]Materials Science and Engineering Program, University of California, San Diego, La Jolla, CA 92093, USA.
*Corresponding author. Email: shqcai@ucsd.edu

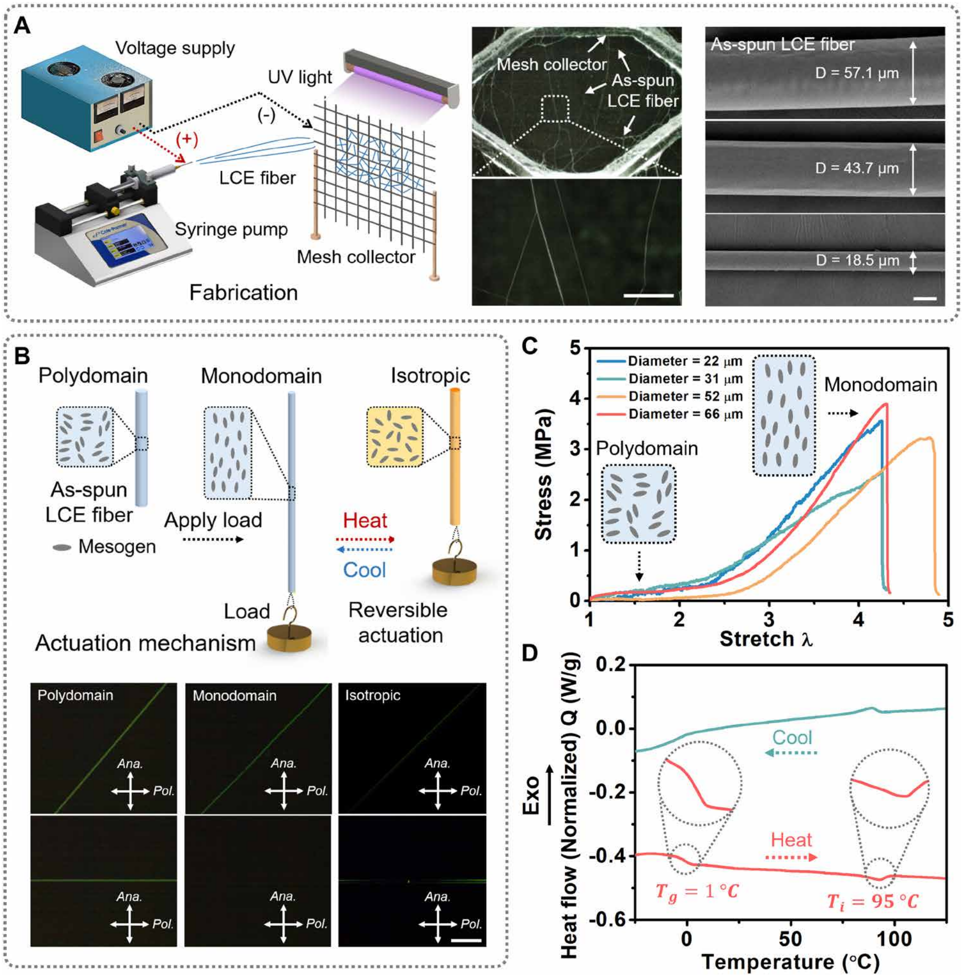

Fig. 1. Fabrication and actuation mechanism of an electrospun LCE microfiber. (**A**) Electrospinning of LCE microfibers. Left: Schematic of the electrospinning setup. The positive electrode of power supply is connected to a metallic needle of the syringe, and the negative electrode is connected to a metallic mesh collector. The syringe pump is used to control the flow rate of the ink with a constant speed. The electrospun LCE microfiber is cross-linked under UV irradiation during the electrospinning. The as-spun LCE microfiber can be collected from the mesh after electrospinning. Middle: Optical images of as-spun LCE microfibers with different diameters on the metal mesh collector. Right: Scanning electron microscopy images of as-spun LCE microfibers with different diameters. (**B**) Top: Actuation mechanism of LCE fiber. The as-spun LCE microfiber is in the polydomain state. When a tensile force is applied onto the fiber, it is stretched from polydomain to monodomain state, and liquid crystal mesogens are aligned along the axial direction. When the stretched LCE microfiber is heated up, it contracts along the axial direction because of the nematic-isotropic transition. The fiber can fully recover to its initial length when it is cooled down. Bottom: POM images of polydomain, monodomain, and isotropic states of LCE microfibers observed at two different angles with respect to the analyzer. (**C**) Uniaxial tensile tests (at 25°C) of as-spun LCE microfibers with different diameters (22 to 66 μm). For the as-spun LCE microfibers with different diameters, the stress remains small when the stretch λ is less than 2.5 and then gradually increases with stretch for larger deformation. The stress plateau corresponds to the rotation of liquid crystal mesogens in the fiber. (**D**) DSC trace of as-spun LCE microfiber. The glass transition temperature T_g of the LCE microfiber is around 1°C, and the nematic-isotropic phase transition temperature T_i is around 95°C. Scale bars, 200 μm [(A), middle], 20 μm [(A), right], and 200 μm [(B), bottom].

fiber when it was observed at 45° or 90° with respect to the analyzer. When the as-spun LCE microfiber was stretched by a uniaxial mechanical force (Fig. 1B, top), the liquid crystal mesogens were aligned along the axial direction. We could observe the maximal brightness of the fiber at 45° and minimal brightness at 90° with respect to the analyzer (Fig. 1B). As shown in Fig. 1B (top), when a stretched LCE microfiber (monodomain) was heated above its phase transition temperature, the LCE microfiber could transit from the nematic phase to isotropic phase, inducing large uniaxial contraction. When the LCE microfiber was cooled down, it could fully recover to its original length (Fig. 1B).

Figure 1C shows the stress-stretch diagram of the as-spun LCE microfibers with different diameters, exhibiting the characteristic of soft elasticity (namely, the flat plateau in the stress-stretch curves). The stress plateau regime corresponds to the rotation of the mesogens. Compared with the bulk LCE obtained from the same synthesis, the strength of LCE fiber is much higher than that of its bulk counterpart, mainly because of the elimination of defects in the material and the small size (fig. S3). Figure 1D shows the differential scanning calorimetry (DSC) measurement of the electrospun LCE fiber, from which we can find that the glass transition temperature and nematic-isotropic phase transition temperature of the fiber are around 1° and 95°C, respectively.

Actuation performance of electrospun LCE microfibers

To systematically characterize the actuation performance of the electrospun LCE microfibers, we applied a tensile force on the fiber and measured its length change as a function of temperature as shown in Fig. 2A. At room temperature (RT = 20°C), the length of LCE microfiber increased from *L* to *l*(RT) because of the applied tensile force. When the environmental temperature was gradually increased to *T*, the LCE microfiber generated uniaxial contraction due to the nematic-isotropic phase transition, and its length decreased from *l*(RT) to *l*(*T*). We then defined the actuation strain as $\varepsilon = \frac{l(\mathrm{RT})-l(T)}{l(\mathrm{RT})} \times 100\%$. The actuation strain of the LCE microfiber as a function of temperature is plotted in Fig. 2B and fig. S4, where the actuation strain of the fiber increases monotonically with temperature. The actuation strains were 55, 33, and 30% at 120°C when the applied stresses were 0.02, 0.08, and 0.16 MPa, respectively. If the as-spun LCE microfiber is not subjected to mechanical load, then the actuation strain is almost negligible, which further confirms that the as-spun fiber is in polydomain state (fig. S5). Moreover, we also studied the actuation strain of LCE microfibers with different diameters, which is shown in Fig. 2C. For a given applied stress, there is no substantial difference of the actuation strain when the diameter changes.

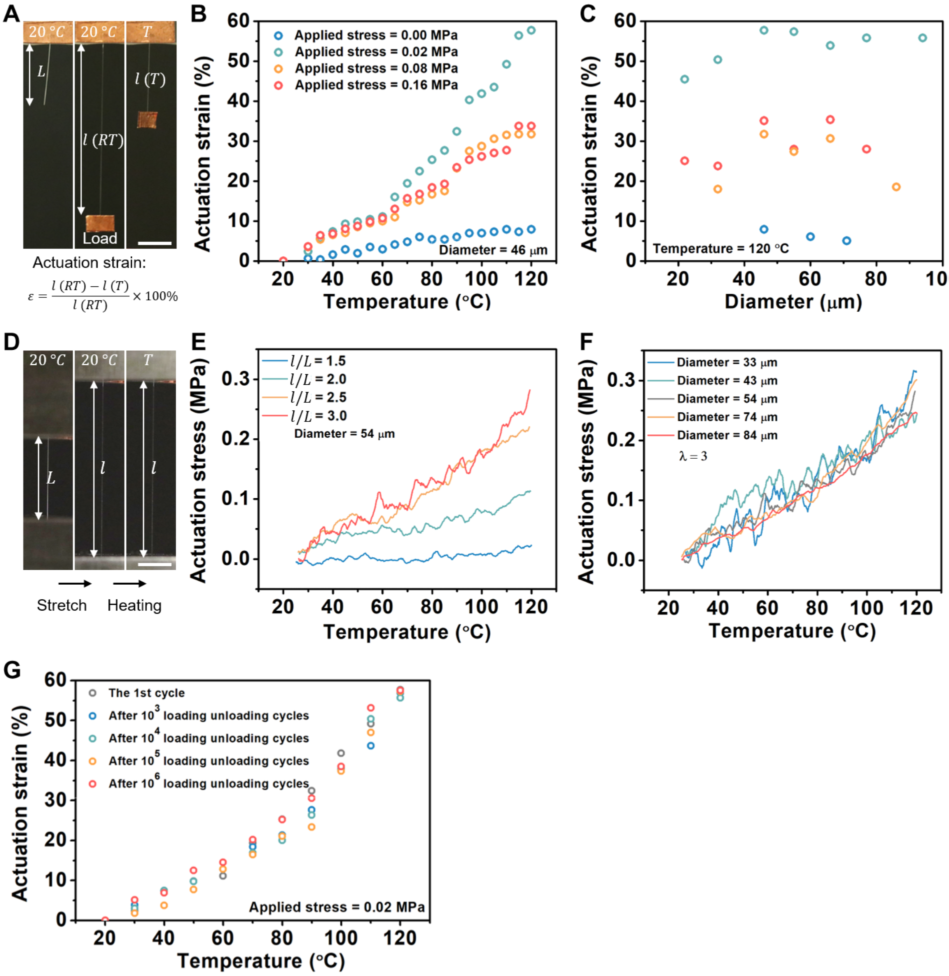

Fig. 2. Actuation performance of electrospun LCE microfibers. (**A**) The length of LCE microfiber in polydomain, monodomain, and isotropic states. The length of the as-spun LCE microfiber (in polydomain state) is denoted by *L*. When a tensile force is applied to the as-spun LCE microfiber, the length of the fiber increases to *l*(RT), and the fiber changes to a monodomain state. The length of the fiber reduces to *l*(*T*) when the temperature is increased to *T*, because of the nematic-to-isotropic phase transition. The actuation strain is defined as $\varepsilon = \frac{l(\mathrm{RT}) - l(T)}{l(\mathrm{RT})} \times 100\%$. (**B**) Actuation strain of electrospun LCE microfiber versus temperature under four different levels of applied stresses (0.00, 0.02, 0.08, and 0.16 MPa). The actuation strain increases monotonically with the temperature. (**C**) The actuation strain of the LCE microfiber at 120°C with different diameters under four different applied stresses. There is no substantial difference in the actuation strain when the fiber diameter changes. (**D**) Actuation stress measurement of LCE microfibers. The as-spun LCE microfiber is firstly stretched to *l* at 20°C. The length of the fiber (*l*) is then fixed as the temperature is gradually increased from 20°C, during which the actuation stress is measured. (**E**) Actuation stress of the LCE microfibers as a function of temperature with four prestretch ratios (*l*/*L*) as 1.5, 2.0, 2.5, and 3.0. The actuation stress increases as the temperature increases. A larger prestretch ratio results in higher actuation stress. (**F**) The actuation stress of the LCE microfibers with different diameters ranging from 33 to 84 μm. No clear size dependence can be found within the range of the fiber diameters. (**G**) After 10^3, 10^4, 10^5, and 10^6 loading-unloading cycles, the actuation strain of the LCE microfiber remains unchanged. Scale bars, 5 mm (A) and 5 mm (D).

Next, we measured the actuation stress of the LCE microfibers with a fixed length. In the experiments, we first applied a prestretch to a polydomain LCE microfiber at 20°C to align the liquid crystal mesogens. After the prestretch, the length of the fiber increased from *L* to *l*. With fixing the length of the fiber as *l*, we measured the actuation stress with the increase in the temperature (Fig. 2D and fig. S6). As shown in Fig. 2E, the actuation stress of the LCE microfiber (D = 54 μm before stretching) increased with the temperature. The LCE microfiber with a larger prestretch ratio can generate larger actuation stress at the same temperature. Specifically, when the temperature was 120°C, the actuation stress of LCE microfiber was 0.28, 0.22, 0.11, and 0.02 MPa at l/L = 3.0, 2.5, 2.0, and 1.5, respectively. Such a trend could be attributed to the better alignment of liquid crystal mesogens with larger prestretch. Similarly, we did not observe strong dependence of the actuation stress on the fiber diameter as shown in Fig. 2F.

As an actuator, both the strength and the durability of LCE microfibers are key performance metrics (*32*, *33*). The actuation stress that the electrospun LCE microfibers can generate is already beyond the strength of their bulk counterpart (fig. S7). In addition, the LCE microfiber has shown superior durability. In the experiments, we cyclically loaded and unloaded the LCE microfiber with 20% maximum strain at 90°C. We then measured the actuation strain of the fiber as function of temperature after 10^3, 10^4, 10^5, and 10^6 loading-unloading cycles, as shown in Fig. 2G, where no performance degeneration can be detected.

Although the actuation stress and strain of the LCE fiber do not depend on the fiber diameter, with the decrease in the diameter, LCE microfiber indeed exhibits faster thermal actuation speed. To estimate the response speed of the LCE microfiber, in the experiment, we used a cartridge heater (surface temperature around 300°C) to heat up the specimen. When the heater approached the fiber (with a distance around 1 mm), it contracted instantaneously (<0.2 s) as shown in movie S1. The LCE microfiber could immediately recover (<0.2 s) to its initial shape when we removed the heat source, as shown in fig. S8.

Self-oscillation of an LCE microfiber in a steady temperature field

Although the electrospun LCE microfibers can respond to temperature change rapidly, varying the temperature of the fiber very quickly is difficult in practical applications. Autonomous oscillation driven by a steady stimulus can be broadly seen in nature and has been recently intensively explored in engineering systems (*34*–*37*). The most salient advantage of a self-oscillating structure is that it does not need periodical on/off control of external stimulus. Here, we demonstrate that a loaded LCE microfiber can self-oscillate in a steady temperature field, because of its thermo-mechanical coupling effect.

In the experiment, we hung an LCE microfiber (D = 33 μm before stretching) in a chamber (Fig. 3A). A homemade electrical heating wire was placed on the bottom of the chamber, and therefore, the temperature in the chamber decreased from the bottom to the top. The temperature distribution in the chamber measured by IR camera is shown in Fig. 3B. Once the fiber is placed into the chamber, it contracts and recovers cyclically and rapidly. The thermally driven self-oscillation can be understood as following: As the end of the LCE fiber gets close to the heating wire, it can be instantaneously heated up and contracts rapidly. Such contraction makes the fiber move away from the heating source, causing the cooling down and length recovery of the fiber, which, in turn, induces the heating up and contraction of the fiber. Figure 3C shows the sequential frames of an LCE microfiber within 1 s. Quantitative measurements of the entire oscillation are shown in Fig. 3D and movie S2. The LCE fiber exhibits a fully reversible and continuous actuation in a chaotic fashion. The maximum actuation strain of LCE microfiber during the oscillation decreases from 55 to 15% when the applied stress increases from 0.02 to 0.16 MPa. We further analyze the data from Fig. 3D by performing the Fourier transformation. The power spectrum density of the actuation strain signal is given in Fig. 3E, which shows that the self-oscillation is chaotic. We postulate that such chaotic oscillation results from the coupling between the airflow in the chamber and the nonlinear thermomechanical behaviors of the LCE fiber (*21*, *38*). Quantitatively modeling the chaotic oscillation of the LCE fiber requires substantial efforts, which is beyond the scope of the current study.

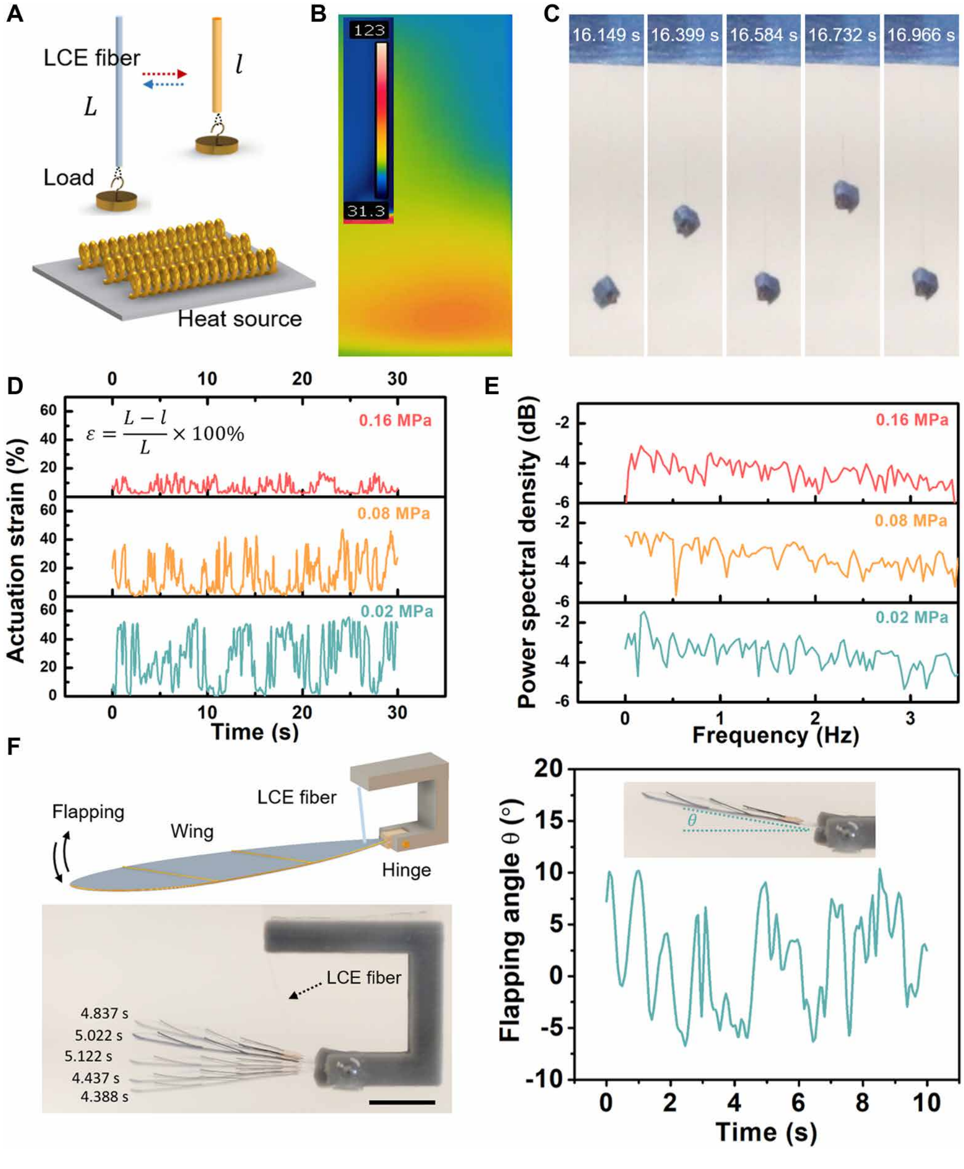

Fig. 3. Self-oscillation of an LCE microfiber in a steady temperature field. (**A**) Schematic illustration of self-oscillation of an LCE microfiber in a steady temperature field. (**B**) Thermal image of the temperature field in the chamber measured by an IR camera. (**C**) Frames from the video (movie S2) of the oscillation of an LCE microfiber (16 to 17 s). (**D**) Actuation strains ($\varepsilon = \frac{L-l}{L} \times 100\%$) of LCE microfiber during the oscillation with three different levels of applied stresses (0.02, 0.08, and 0.16 MPa). (**E**) Frequency spectra of the actuation strain time series shown in (D). (**F**) Autonomous wing flapping actuated by an LCE microfiber in a steady temperature field. Scale bar, 10 mm (F).

Although several self-oscillating LCE structures have been designed and fabricated, most of them are triggered by light via self-shadowing effect (*35*, *39*). The self-oscillation of LCE microfibers driven by a steady temperature gradient demonstrated in the current work may have the potential to harvest energy from low-quality waste heat. The LCE microfiber can be also used to construct self-propelling devices in an environment with temperature gradients. Figure 3F and movie S3 show cyclical wing flapping driven by a LCE microfiber in a steady but inhomogeneous temperature field. In the experiment, we hung a wing at the bottom of an LCE microfiber. The wing could flap continuously in a steady temperature field, driven by the self-oscillation of the LCE microfiber.

Light-controlled actuation of electrospun LCE microfibers

Because of the small diameter, applying external stimuli to trigger the actuation of a single LCE microfiber can be difficult. To achieve controllable actuation of LCE microfibers, we coated a polydopamine (PDA) layer on the surface of the fiber to make it light responsive through photothermal effects. Previous studies have demonstrated that PDA coating can convert light to heat with high efficiency in the NIR region (*40*). In addition, it has been shown that thin PDA layers can easily adhere on the surfaces of many different materials (*41*, *42*).

In the experiments, we fabricated PDA-coated LCE microfibers through a simple dip-coating process, during which the fiber (prestretched monodomain state) was submerged in a dopamine/tris buffer solution as shown in Fig. 4A. After 48 hours, the surface of LCE fiber turned into a dark gray color, indicating successful polymerization of dopamine on the surface of the LCE microfiber.

The PDA-coated LCE microfiber can generate longitudinal contraction under the exposure of NIR light due to the photothermal effect as shown in Fig. 4B. In the experiment, to precisely control the frequency of NIR light exposure, a rotating motor connected with a half opening mask was used as shown in Fig. 4B. To evaluate the actuation performance of PDA-coated LCE microfiber under the periodic illumination of NIR light, laser beams with two different levels of power were used in the experiments, as shown in fig. S9A. When the NIR light was exposed to the PDA-coated LCE fiber (D = 35 μm), the actuation strain of LCE fiber reached the maximum value within 0.1 s. The PDA-coated LCE fiber could rapidly recover to its initial length within 0.1 s when the NIR light was blocked by the rotating mask. The laser with high power (4000 mW/cm^2) could induce larger actuation in the LCE fiber (20%) than the one with lower power (2000 mW/cm^2). In addition, we had also measured the response speed of PDA-coated LCE microfibers with different diameters as shown in fig. S9B. The fiber with the smallest diameter exhibited both the fastest actuation and recovery speed.

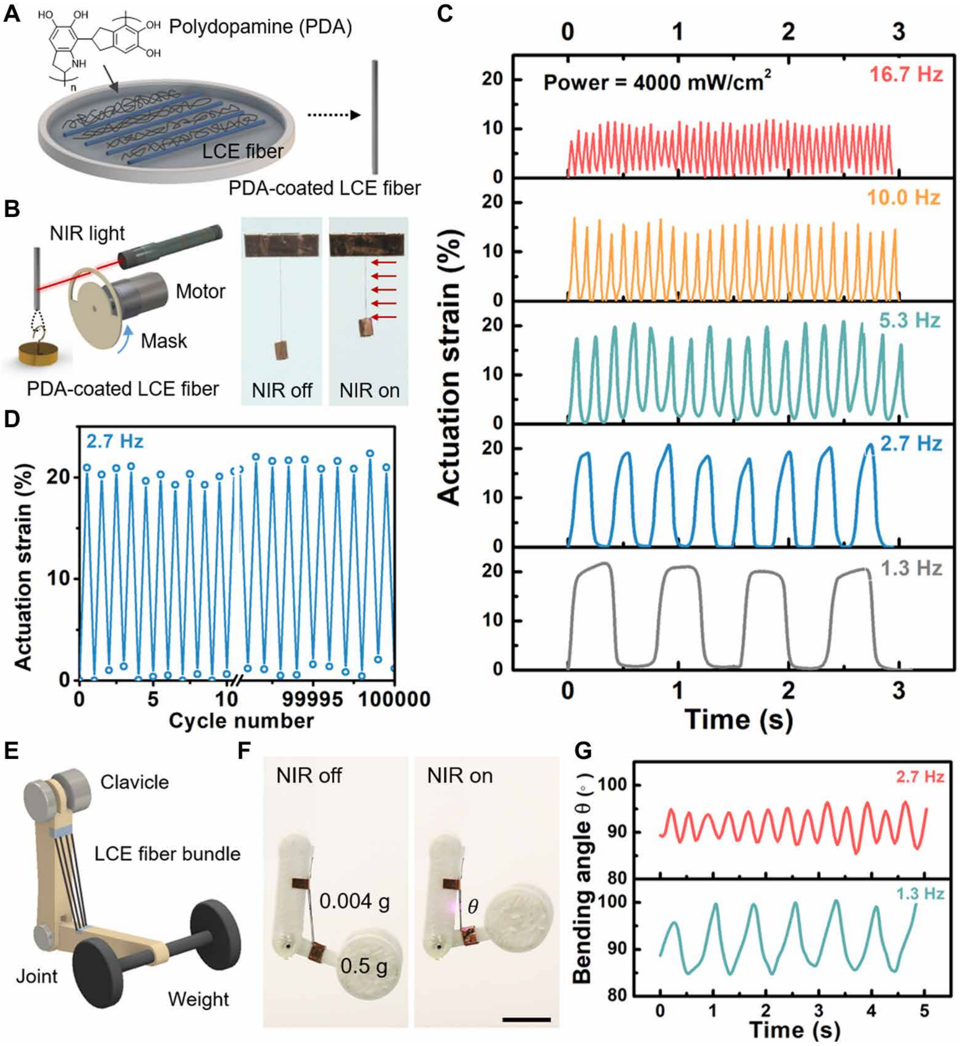

Fig. 4. Laser-powered actuation of PDA-coated LCE microfibers. (**A**) Preparation of PDA-coated LCE microfibers via dip-coating method. (**B**) When a PDA-coated LCE microfiber is exposed to a NIR light, it contacts and lifts up a weight. The frequency of NIR light illumination can be controlled by the rotation speed of the motor attached with a half-opening mask. (**C**) Influence of NIR light illumination frequency on the actuation strain of a PDA-coated LCE microfiber. The maximum actuation strain decreases with the increase in the light illumination frequency. (**D**) Laser-powered actuation performance of the LCE microfiber remains the same after 10^5 cycles of periodical light illumination. (**E**) Schematic of weight-lifting artificial arm. An LCE microfiber bundle can be implemented as a bicep artificial muscle. (**F**) When the fiber bundle is exposed to a NIR light, the bicep contracts, which causes the arm to bend. (**G**) Elbow bending angle as a function of time for two different frequencies of light illumination. Scale bar, 10 mm (F).

We further studied the actuation performance of PDA-coated LCE microfiber (D = 35 μm) under a different frequency of NIR light exposure (4000 mW/cm^2). By controlling the rotation speed of the motor, the frequency of NIR light exposure could be varied from 1.3 to 16.7 Hz. As shown in Fig. 4C and movie S4, at a low frequency of 1.3 Hz, the actuation strain increased with time nearly to a plateau value (20%) and then decreased to zero. When we increased the frequency to the range of 2.7 to 5.3 Hz, the maximum actuation strain remained 20%. However, at higher frequencies of light exposure of 10.0 and 16.7 Hz, the maximum actuation strain of a PDA-coated LCE microfiber decreased to 15 and 10%, respectively.

Figure 4D further shows that under a periodic NIR laser illumination, a PDA-coated LCE microfiber with the diameter of 35 μm can lift up and lower down a weight over 10^5 cycles. With the applied tensile stress of 0.16 MPa, the maximum actuation strain of the fiber remained 20% without any degradation. The bulk LCE obtained from the same synthesis, however, can only survive for nine cycles with same loading condition because of its poor fatigue properties (fig. S10).

A single fiber can only produce small actuation force, which may not be sufficient for applications. To overcome this limitation, we assembled multiple LCE microfibers to amplify the actuation force. As shown in fig. S11, a single fiber (D = 68 μm) could lift a 0.1-g weight, whereas four such fibers in parallel could lift a weight around 0.5 g without affecting the response speed (movies S5 and S6). We then attached the PDA-coated LCE microfiber bundle, mimicking a bicep muscle, to a 3D-printed arm skeleton to realize fast elbow movements (Fig. 4E). When the fiber bundle was exposed to NIR light, it contracted, causing the arm to bend and lift up a weight of 0.5 g (Fig. 4F). The PDA-coated LCE microfiber bundle could fully recover to its original state when the NIR light was switched off. In Fig. 4G, we show the change of the bending angle of the elbow with time under periodical illumination of a NIR light (movie S7).

Comparisons between the electrospun LCE microfiber actuator and other existing fiber actuators

In terms of the magnitude of actuation strain (>50%), actuation stress (0.3 MPa), response speed (300%/s), and work density (20 kJ/m^3), the LCE microfibers exhibit a performance comparable to human muscle (fig. S12) (*32*, *33*). In the Ashby plot shown in Fig. 5A, we collect the actuation strain and strain rate of different fiber actuators reported in the literature.

In robotics applications, power density is one of the key performance metrics of an actuator. The actuation power density of an LCE fiber can be estimated as $P = \sigma\varepsilon/\rho\tau$, where σ is the applied stress, ε is the actuation strain, τ is the characteristic time for heating up or cooling down the fiber, and ρ is the mass density. The magnitude of $\sigma\varepsilon$ (work density) and the mass density of the LCE material have weak size dependence. Therefore, reducing the characteristic time τ is the key to increase the power density of the LCE fiber.

In the current work, we fabricated LCE fibers with small diameters through electrospinning method to decrease the characteristic time τ. In the experiments above, we have demonstrated two different ways of heating up and cooling down the LCE fibers. For the first method, we used environmental heating and natural cooling to heat up and cool down the fiber. Because of the small diameters of the fibers, the characteristic heating or cooling time for the fibers is determined by the thermal time constant: $\tau = d\rho c/h$, where d is the fiber diameter, c is gravimetric specific heat capacity, and h is the convection coefficient. Using the representative numbers for the LCE fiber and the environment, we can obtain that $\tau \sim 1$ s (with $d \sim 10$ μm, $\rho \sim 10^3$ kg/m^3, $c \sim 10^3$ J/kg·K, and $h \sim 10$ W/m^2·K), which is consistent with the experimental results shown in Fig. 3D. However, in the applications, this characteristic time constant of heating or cooling the LCE is often much smaller than the time needed to change the environmental temperature near the fiber. Therefore, in the applications, the response time of the LCE fiber will be more likely determined by the time needed to change the environmental temperature. For the second method, we adopted photothermal mechanism to heat up or cool down the LCE fibers coated by a PDA layer. For this method, the conversion of light to heat almost needs no time. Therefore, the time scale of the LCE fiber to contract (by laser heating) and recover back (through air cooling) is given by the thermal time constant: $\tau \sim 1$ s. On the basis of the results plotted in Fig. 4C, we estimate that the power density of the LCE microfiber is 400 W/kg. The Ashby plot in Fig. 5B shows the comparisons of the power density and actuation strain rate of LCE microfiber actuator and other LCE actuators reported in the literature.

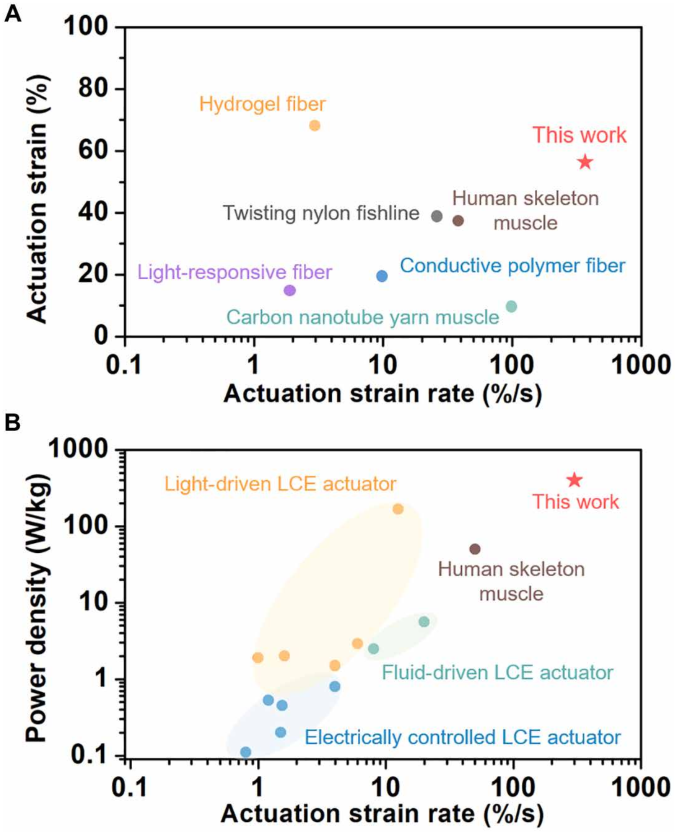

Fig. 5. Comparisons between the electrospun LCE microfiber and other actuators. (**A**) Ashby plot of actuation strain versus actuation strain rate of fiber actuators including twisting nylon fishline (*6*), conductive polymer fiber (*48*), light-responsive fiber (*50*), hydrogel fiber (*52*), carbon nanotube yarn muscle (*53*), and human skeleton muscle (*33*). (**B**) Ashby plot of power density versus actuation strain rate of LCE-based soft actuators and human skeleton muscle.

Applications of LCE microfiber actuator

We constructed microdevices using electrospun LCE microfiber actuators for proof-of-concept demonstration. First, we designed and fabricated an electrically controlled microtweezer actuated by LCE microfiber. An electrically controlled soft actuator allows its easy integrations with low-cost electronic devices and convenient programmability, which is highly desired for micromanipulation systems and devices (*43*, *44*). As shown in Fig. 6A, several LCE microfibers connected the two beams near their tips, and two microheaters were attached to the inner sides of the beam. When a voltage was applied to the microheaters, the temperature near them increased, triggering the contraction of the LCE microfiber and the close of the two tips of the microtweezer (Fig. 6B and movie S8). The two tips of the microtweezer reopened when the voltage was turned off. The displacement of the tips could be easily controlled by the applied voltage, as shown in Fig. 6C. Compared with most existing fiber actuators, the small weight, large actuation strain, and fast response are the advantages of the LCE microfiber actuator for the microtweezer application.

Light-driven LCE microfibers can be rapidly and remotely controlled, which makes them a great choice for building untethered microrobots (*45*). Here, we fabricated a microswimmer based on a PDA-coated LCE microfiber as shown in Fig. 6D. The microswimmer is mainly composed of flexible hinges, polyimide tapes (with curved end), polyethylene terephthalate (PET) films, and a PDA-coated LCE microfiber. Although the density of the PET film (1.38 g/cm^3) is larger than that of the water, the microswimmer could surf on the water surface because of the capillary force (Fig. 6D). The microswimmer could move rapidly on the surface of water driven by a NIR laser, as shown in Fig. 6E. For one swimming stroke, when the LCE fiber was exposed to the NIR laser, the fiber contracted, causing the hinge to fold. As a result, the front fin moved upward and pushed the water backward, which could generate a thrust force to make the entire body to move forward. The movement of robot was negligible

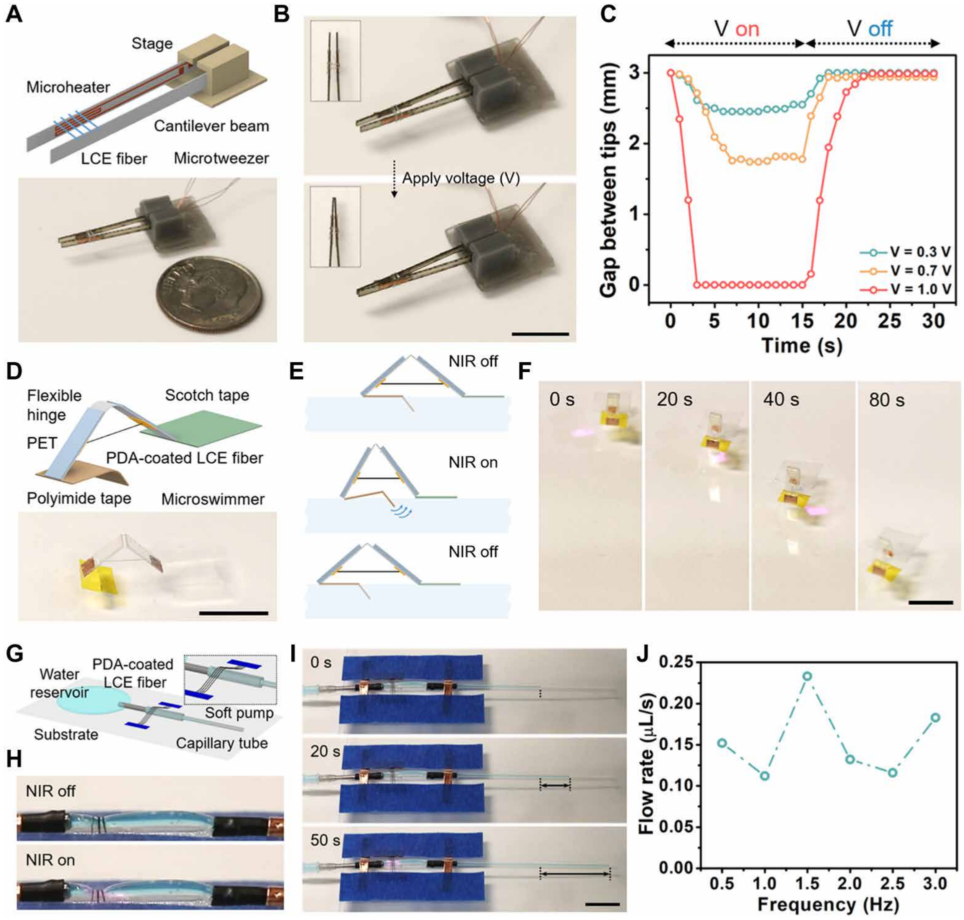

Fig. 6. Applications of electrospun LCE microfiber actuators. (**A**) Schematic and photo of a microtweezer. The microtweezer is composed of two cantilever beams (equipped with microheater at the inner side), a stage, and LCE microfibers. The LCE microfibers are mounted near the tip of two cantilever beams. (**B**) Working mechanism of the microtweezer. When a voltage is applied onto the two heaters, the LCE microfibers can be heated up and contract, which makes the tips of the tweezer close. (**C**) Tip displacement of microtweezer versus time for three different voltages: 0.3, 0.7, and 1.0 V. (**D**) Schematic and a photo of a microswimmer. The microswimmer is mainly composed of a flexible hinge, PET films, polyimide tape, and an LCE microfiber. (**E**) Schematic illustration of the microswimmer during light-powered swimming. When the LCE microfiber is exposed to the NIR light, the fiber contracts, so the front fin moves upward and pushes the water backward, which generates thrust force making entire body move forward. (**F**) Frames from the video (movie S9) of light-powered swimming of the microswimmer. (**G**) Schematic of a soft impedance pump. Three PDA-coated LCE microfibers are placed across a soft tube and anchored on the substrate. A metallic needle connects the soft tube and a water reservoir. Another glass capillary tube is connected to the other end of the soft tube. (**H**) When NIR light is applied onto the PDA-coated LCE microfibers, the soft tube deforms and the water inside of the soft tube is pumped from the water reservoir to the capillary tube. (**I**) Frames from the videos of the soft pump with the light illumination at a frequency of 1.0 Hz. (**J**) The flow rate of soft pump versus the frequency of the light illumination. Scale bars, 10 mm (B, D, F, and I).

when the NIR light was switched off. With the NIR light switching on and off periodically, the microswimmer could generate a large displacement on the surface of the water, as shown in Fig. 6F and movie S9. Building a light-controlled microrobot requires actuators that generate fast actuation with large actuation strain and stress. We believe that more complex design and fabrication will be needed to a construct a similar microrobot by using other fiber actuators.

Finally, we fabricated a soft micro-impedance pump driven by PDA-coated LCE microfibers (Fig. 6G). The soft impedance pump is composed of a soft tube in the middle connected to two rigid tubes. Three PDA-coated LCE microfibers were covered across the soft tube and anchored on the substrate as shown in Fig. 6 (G and H). Cyclic light-induced contraction of the LCE fibers caused periodic local squeezing the soft tube as shown in Fig. 6H. Because the position of the LCE fibers is not in the middle of the soft tube, the periodic squeezing can continuously pump the water from one end to the other as shown in Fig. 6I and movie S10. The flow rate of the soft impedance pump is shown in Fig. 6J. The flow rate of the light-powered micropump demonstrated in the current work is comparable to that of some previous studies using piezoelectric actuators powered by electricity (*46*).

Thanks to the contactless manner and high spatial/temporal resolution, light illumination has been widely recognized as an excellent way to control microfluidic devices (*47*). To construct an efficient light-powered microfluid pump, fast optically driven actuation and a combination of large actuation strain and stress of the fiber actuator are necessary. It is very challenging to use previously developed fiber-based actuators to construct a light-powered microfluidic pump with the performance comparable to what has been demonstrated (Fig. 6J).

DISCUSSION

In the recent few years, various fiber actuators have been fabricated with great performance. However, all of those fiber actuators still have certain limitations for applications. Many of those fiber actuators are thermally driven, such as twisted nylon fishline, conductive polymer fiber (*6*, *48*), and shape memory alloy fibers (*49*). Several recently developed optically responsive fiber actuators can generate multidirectional bending and uniaxial contraction based on the photochemical or photothermal mechanism (*50*, *51*). However, the responses of all those fiber actuators are slow because of their large sizes. The fiber actuators made from responsive hydrogels respond even slower, because solvent diffusion is required (*52*). Carbon nanotube yarn muscle can generate fast actuation rate (100%/s), but its actuation strain is small (typically less than 5%) (*53*).

Here, we designed and fabricated a LCE microfiber actuator through a facile electrospinning technique. We have conducted systematic characterizations of the actuation performance of the microfiber actuator. The electrospun LCE microfiber actuator exhibited similar performance as human muscle fibers in terms of the actuation strain, stress, response speed, work density, and power density. Thanks to the small diameter, the LCE microfibers also exhibited high strength and superior durability. To make the LCE fiber responsive to light, we coated a thin PDA layer on the surface of the fiber through a simple dip-coating method. In terms of the practical applications, we demonstrated the feasibility of using the LCE microfiber actuator to construct versatile microrobots and a microfluidic pump. Our work may open up an avenue to build soft robotics or soft machines using LCEs as the actuator.

Last, it is also worth mentioning that the diameter of the LCE fibers made from electrospinning varies greatly (10 to 100 μm), which may not be desired in practical applications. In the current work, we manually select the LCE fibers with the diameter of our interest. Additional efforts will be needed to obtain electrospun LCE microfiber actuators with more uniform diameters. Moreover, the smallest diameter of the current electrospun LCE fiber in the current work is around 10 μm. Reducing the diameter of LCE microfiber can further enhance the responsive speed, which may be realized by tuning the electrospinning parameters.

MATERIALS AND METHODS

Materials

{1,4-Bis-[4-(3-acryloyloxypropyloxy) benzoyloxy]-2-methylbenzene} (RM257) (Wilshire Company, 95%), (2-hydroxyethoxy)-2-methylpropiophenone (HHMP; Sigma-Aldrich, 98%), HDT (Alfa Aesar, 97%), dipropylamine (DPA; Sigma-Aldrich, 98%), dopamine hydrochloride (99%, Alfa Aesar), tris base (Thermo Fisher Scientific), chloroform, and methylene chloride were used as received without further purification.

Synthesis of the LCE ink for electrospinning

RM257 (12.95 g, 22 mmol) was dissolved in 50 ml of CH_2Cl_2. Then, HDT (3.006 g, 20 mmol) and catalyst DPA (0.200 g, 2 mmol) were added dropwise into the solution. The solution was stirred at RT for 12 hours. Then, the solvent was evaporated and the product was obtained after being dried at 80°C in the oven overnight. Last, we dissolved the product into chloroform; the concentration of the ink was set to be 20 weight % (wt %). We then added 5 wt % HHMP into the ink and stirred for 12 hours.

Fabrication of LCE microfiber

The schematic of electrospinning setup is shown in Fig. 1A. The LCE ink was first loaded into a 1-ml plastic syringe with a 16-gauge industrial needle. Then, we used the syringe pump (Cole-Parmer, USA) to precisely control the flow rate from the needle with a speed of 0.02 ml/min. A metal mesh with hexagonal gap was used to collect the electrospun LCE microfibers. The positive electrode of the power source was connected to the tip of the needle; the negative electrode of the power source was connected to the metal mesh. The applied voltage was set to 6 kV. During the electrospinning, the LCE microfibers were exposed under UV irradiation to finish the cross-link process. The time for the electrospinning was 2, 5, and 15 min to obtain LCE microfibers with different quantities and diameters; the diameter distribution is shown in fig. S2. After electrospinning, the as-spun LCE microfiber can be cut using scissors.

Fabrication of PDA-coated LCE microfiber

The dopamine hydrochloride (0.2 g, 1.05 mmol) and tris base (0.1 g, 0.83 mmol) were dissolved into 100 ml of water. Then, the monodomain LCE microfibers were immersed into the solution for 48 hours. The pH value of the tris base buffer was set to be 8.5. The fibers became dark gray color after submerging. Then, the resultant PDA-coated LCE microfibers were washed using water.

Morphology characterization of LCE microfiber

The diameters of LCE microfibers were measured under both optical microscope (Zeiss) and scanning electron microscope (Zeiss Sigma 500). The alignment of the LCE microfiber can be characterized by polarized optical microscope (Zeiss).

Uniaxial tension tests of as-spun LCE microfiber with different diameters

The force-displacement relationship of as-spun LCE microfiber can be measured using a micromechanical tester (Modular Force Stage, Linkam instrument) equipped with a 2-N loading cell (force resolution, ~0.00001 N). The initial length of an as-spun LCE microfiber is 10 mm. The loading speed is set to be 0.1 mm/s. After measurements, the stress was equal to the force divided by initial cross-sectional area. The strain was equal to the displacement divided by initial length. The stress-strain relationship can be found in Fig. 1C.

DSC measurement of as-spun LCE microfiber

The DSC measurement was conducted using a Discovery DSC 250 (TA instruments) in the nitrogen atmosphere. The 2-mg as-spun LCE microfibers were sealed in the aluminum pans. The heating and cooling scanning rate was 5°C/min in the temperature range between −35° and 150°C.

Actuation strain and stress measurements of LCE microfiber

To measure the actuation strain, the fiber (with external load) was placed into the high-temperature testing chamber (LRHS-100, Shanghai Linpin Instrument Stock Co Ltd). At each temperature, we waited for 5 min until the temperature inside of the chamber was stable. Then, we used a digital camera (Canon 80D) to capture the image. We characterized the length and the actuation strain of LCE microfiber at each temperature by analyzing the images, using ImageJ. The results are shown in figs. S4 and S5.

To measure the actuation stress, we used a micromechanical tester (Modular Force Stage, Linkam Scientific Instrument) equipped with a 2-N loading cell (force resolution, ~0.00001 N). The device is shown in fig. S6. We first applied prestretch by λ to an as-spun LCE microfiber; the length of the fiber increased from L to l; by fixing the length l, we increased the temperature with 20°C/min heating rate and measured the actuation force. The actuation stress was equal to the force divided by the initial cross-sectional area. The results can be found in Fig. 2 (D to F).

To measure the actuation strain versus time (Fig. 4C) under different frequencies, we characterized it by analyzing the videos taken from a high-speed camera (iX Cameras i-SPEED); then, we used ImageJ to measure the length of LCE microfiber in each frame.

Fabrication of microtweezer, microswimmer, and microsoft impedance pump

We created the microheater using a homemade laser cutting machine and glued the microheater onto the FR4 stripes (20 mm by 3 mm by 0.3 mm). We then glued two cantilever beams to the holder, and a single LCE microfiber was warped around onto the two cantilever beams near the tip. The microtweezer was connected to the power source (Dr. Meter PS-305DM). The fabricated microtweezer is shown in Fig. 6A.

The microswimmer was composed of a foldable structure made from PET film. We glued polyimide tape and Scotch tape at the front and rear sides. A single PDA-coated LCE microfiber was mounted in the middle to trigger the foldable structure. The entire microswimmer is shown in Fig. 6D.

The soft impedance pump was composed of a soft tube (Ecoflex) in the middle, an 18-gauge industrial needle, and a capillary tube at both sides. We used heat-shrink tubes to connect each tube. We placed several PDA-coated LCE microfibers onto the soft tube. All the components were attached to the glass substrate using tape. The microsoft impedance pump is shown in Fig. 6G.

SUPPLEMENTARY MATERIALS

robotics.sciencemag.org/cgi/content/full/6/57/eabi9704/DC1
Materials and Methods
Figs. S1 to S12
Movies S1 to S10

REFERENCES AND NOTES

1. M. Zmyślony, K. Dradrach, J. Haberko, P. Nałęcz-Jawecki, M. Rogóż, P. Wasylczyk, Optical pliers: Micrometer-scale, light-driven tools grown on optical fibers. *Adv. Mater.* **32**, 2002779 (2020).
2. H. Bai, S. Li, J. Barreiros, Y. Tu, C. R. Pollock, R. F. Shepherd, Stretchable distributed fiber-optic sensors. *Science* **370**, 848–852 (2020).
3. T. Jia, Y. Wang, Y. Dou, Y. Li, M. Jung de Andrade, R. Wang, S. Fang, J. Li, Z. Yu, R. Qiao, Z. Liu, Y. Cheng, Y. Su, M. Minary-Jolandan, R. H. Baughman, D. Qian, Z. Liu, Moisture sensitive smart yarns and textiles from self-balanced silk fiber muscles. *Adv. Funct. Mater.* **29**, 1808241 (2019).
4. J. Xiong, J. Chen, P. S. Lee, Functional fibers and fabrics for soft robotics, wearables, and human–robot interface. *Adv. Mater.* 2002640 (2020).
5. X. Duan, J. Yu, Y. Zhu, Z. Zheng, Q. Liao, Y. Xiao, Y. Li, Z. He, Y. Zhao, H. Wang, L. Qu, Large-scale spinning approach to engineering knittable hydrogel fiber for soft robots. *ACS Nano* **14**, 14929–14938 (2020).
6. C. S. Haines, M. D. Lima, N. Li, G. M. Spinks, J. Foroughi, J. D. Madden, S. H. Kim, S. Fang, M. J. De Andrade, F. Göktepe, S. M. Mirvakili, S. Naficy, X. Lepró, J. Oh, M. E. Kozlov, S. J. Kim, X. Xu, B. J. Swedlove, G. G. Wallace, R. H. Baughman, Artificial muscles from fishing line and sewing thread. *Science* **343**, 868–872 (2014).
7. M. Porter, A. Vandervoort, J. Lexell, Aging of human muscle: Structure, function and adaptability. *Scand. J. Med. Sci. Sports* **5**, 129–142 (1995).
8. J. J. Feher, *Quantitative Human Physiology: An Introduction* (Academic Press, 2017).
9. S. Methenitis, N. Karandreas, K. Spengos, N. Zaras, A.-N. Stasinaki, G. Terzis, Muscle fiber conduction velocity, muscle fiber composition, and power performance. *Med. Sci. Sports Exerc.* **48**, 1761–1771 (2016).
10. R. Bottinelli, M. Pellegrino, M. Canepari, R. Rossi, C. Reggiani, Specific contributions of various muscle fibre types to human muscle performance: An in vitro study. *J. Electromyogr. Kinesiol.* **9**, 87–95 (1999).
11. M. Warner, E. M. Terentjev, *Liquid Crystal Elastomers* (Oxford Univ. Press, 2007), vol. 120.
12. T. J. White, D. J. Broer, Programmable and adaptive mechanics with liquid crystal polymer networks and elastomers. *Nat. Mater.* **14**, 1087–1098 (2015).
13. Q. He, Z. Wang, Y. Wang, A. Minori, M. T. Tolley, S. Cai, Electrically controlled liquid crystal elastomer–based soft tubular actuator with multimodal actuation. *Sci. Adv.* **5**, eaax5746 (2019).
14. Q. He, Z. Wang, Z. Song, S. Cai, Bioinspired design of vascular artificial muscle. *Adv. Mater. Technol.* **4**, 1800244 (2019).
15. Q. He, Z. Wang, Y. Wang, Z. Song, S. Cai, Recyclable and self-repairable fluid-driven liquid crystal elastomer actuator. *ACS Appl. Mater. Interfaces* **12**, 35464–35474 (2020).
16. C. P. Ambulo, J. J. Burroughs, J. M. Boothby, H. Kim, M. R. Shankar, T. H. Ware, Four-dimensional printing of liquid crystal elastomers. *ACS Appl. Mater. Interfaces* **9**, 37332–37339 (2017).
17. T. H. Ware, M. E. McConney, J. J. Wie, V. P. Tondiglia, T. J. White, Voxelated liquid crystal elastomers. *Science* **347**, 982–984 (2015).
18. M. J. Ford, C. P. Ambulo, T. A. Kent, E. J. Markvicka, C. Pan, J. Malen, T. H. Ware, C. Majidi, A multifunctional shape-morphing elastomer with liquid metal inclusions. *Proc. Natl. Acad. Sci.* **116**, 21438–21444 (2019).
19. Z. Wang, Z. Wang, Y. Zheng, Q. He, Y. Wang, S. Cai, Three-dimensional printing of functionally graded liquid crystal elastomer. *Sci. Adv.* **6**, eabc0034 (2020).
20. D. J. Roach, C. Yuan, X. Kuang, V. C.-F. Li, P. Blake, M. L. Romero, I. Hammel, K. Yu, H. J. Qi, Long liquid crystal elastomer fibers with large reversible actuation strains for smart textiles and artificial muscles. *ACS Appl. Mater. Interfaces* **11**, 19514–19521 (2019).
21. J. Naciri, A. Srinivasan, H. Jeon, N. Nikolov, P. Keller, B. R. Ratna, Nematic elastomer fiber actuator. *Macromolecules* **36**, 8499–8505 (2003).
22. X. Pang, L. Qin, B. Xu, Q. Liu, Y. Yu, Ultralarge contraction directed by light-driven unlocking of prestored strain energy in linear liquid crystal polymer fibers. *Adv. Funct. Mater.* **30**, 2002451 (2020).
23. Z.-M. Huang, Y.-Z. Zhang, M. Kotaki, S. Ramakrishna, A review on polymer nanofibers by electrospinning and their applications in nanocomposites. *Compos. Sci. Technol.* **63**, 2223–2253 (2003).
24. J. D. Schiffman, C. L. Schauer, A review: Electrospinning of biopolymer nanofibers and their applications. *Polym. Rev.* **48**, 317–352 (2008).
25. Q. He, Z. Wang, Y. Yan, J. Zheng, S. Cai, Polymer nanofiber reinforced double network gel composite: Strong, tough and transparent. *Extreme Mech. Lett.* **9**, 165–170 (2016).
26. I. S. Chronakis, Novel nanocomposites and nanoceramics based on polymer nanofibers using electrospinning process—A review. *J. Mater. Process. Technol.* **167**, 283–293 (2005).
27. J. Matulevicius, L. Kliucininkas, D. Martuzevicius, E. Krugly, M. Tichonovas, J. Baltrusaitis, Design and characterization of electrospun polyamide nanofiber media for air filtration applications. *J. Nanomater.* **2014**, 859656 (2014).
28. M. Zhu, J. Han, F. Wang, W. Shao, R. Xiong, Q. Zhang, H. Pan, Y. Yang, S. K. Samal, F. Zhang, C. Huang, Electrospun nanofibers membranes for effective air filtration. *Macromol. Mater. Eng.* **302**, 1600353 (2017).
29. Q. P. Pham, U. Sharma, A. G. Mikos, Electrospinning of polymeric nanofibers for tissue engineering applications: A review. *Tissue Eng.* **12**, 1197–1211 (2006).
30. J. M. Deitzel, J. Kleinmeyer, D. Harris, N. B. Tan, The effect of processing variables on the morphology of electrospun nanofibers and textiles. *Polymer* **42**, 261–272 (2001).
31. S. Ramakrishna, *An Introduction to Electrospinning and Nanofibers* (World Scientific, 2005).
32. J. D. Madden, N. A. Vandesteeg, P. A. Anquetil, P. G. Madden, A. Takshi, R. Z. Pytel, S. R. Lafontaine, P. A. Wieringa, I. W. Hunter, Artificial muscle technology: Physical principles and naval prospects. *IEEE J. Ocean. Eng.* **29**, 706–728 (2004).
33. S. M. Mirvakili, I. W. Hunter, Artificial muscles: Mechanisms, applications, and challenges. *Adv. Mater.* **30**, 1704407 (2018).
34. M. Hua, C. Kim, Y. Du, D. Wu, R. Bai, X. He, Swaying gel: Chemo-mechanical self-oscillation based on dynamic buckling. *Matter* **4**, 1029–1041 (2021).
35. S. Serak, N. Tabiryan, R. Vergara, T. J. White, R. A. Vaia, T. J. Bunning, Liquid crystalline polymer cantilever oscillators fueled by light. *Soft Matter* **6**, 779–783 (2010).
36. K. Kumar, C. Knie, D. Bléger, M. A. Peletier, H. Friedrich, S. Hecht, D. J. Broer, M. G. Debije, A. P. H. J. Schenning, A chaotic self-oscillating sunlight-driven polymer actuator. *Nat. Commun.* **7**, 11975 (2016).
37. H. Zeng, M. Lahikainen, L. Liu, Z. Ahmed, O. M. Wani, M. Wang, H. Yang, A. Priimagi, Light-fuelled freestyle self-oscillators. *Nat. Commun.* **10**, 5057 (2019).
38. L. Jin, Z. Zeng, Y. Huo, Thermomechanical modeling of the thermo-order–mechanical coupling behaviors in liquid crystal elastomers. *J. Mech. Phys. Solids* **58**, 1907–1927 (2010).
39. A. H. Gelebart, D. J. Mulder, M. Varga, A. Konya, G. Vantomme, E. Meijer, R. L. Selinger, D. J. Broer, Making waves in a photoactive polymer film. *Nature* **546**, 632–636 (2017).
40. Y. Liu, K. Ai, J. Liu, M. Deng, Y. He, L. Lu, Dopamine-melanin colloidal nanospheres: An efficient near-infrared photothermal therapeutic agent for in vivo cancer therapy. *Adv. Mater.* **25**, 1353–1359 (2013).
41. H. Tian, Z. Wang, Y. Chen, J. Shao, T. Gao, S. Cai, Polydopamine-coated main-chain liquid crystal elastomer as optically driven artificial muscle. *ACS Appl. Mater. Interfaces* **10**, 8307–8316 (2018).
42. Z. Li, X. Zhang, S. Wang, Y. Yang, B. Qin, K. Wang, T. Xie, Y. Wei, Y. Ji, Polydopamine coated shape memory polymer: Enabling light triggered shape recovery, light controlled shape reprogramming and surface functionalization. *Chem. Sci.* **7**, 4741–4747 (2016).
43. C. Wang, K. Sim, J. Chen, H. Kim, Z. Rao, Y. Li, W. Chen, J. Song, R. Verduzco, C. Yu, Soft ultrathin electronics innervated adaptive fully soft robots. *Adv. Mater.* **30**, 1706695 (2018).
44. Y. Wang, Z. Wang, Q. He, P. Iyer, S. Cai, Electrically controlled soft actuators with multiple and reprogrammable actuation modes. *Adv. Intell. Syst.* **2**, 1900177 (2020).
45. Z. C. Jiang, Y. Y. Xiao, Y. Zhao, Shining light on liquid crystal polymer networks: Preparing, reconfiguring, and driving soft actuators. *Adv. Opt. Mater.* **7**, 1900262 (2019).
46. D. Rinderknecht, A. I. Hickerson, M. Gharib, A valveless micro impedance pump driven by electromagnetic actuation. *J. Micromech. Microeng.* **15**, 861–866 (2005).
47. D. Baigl, Photo-actuation of liquids for light-driven microfluidics: State of the art and perspectives. *Lab Chip* **12**, 3637–3653 (2012).
48. M. Kanik, S. Orguc, G. Varnavides, J. Kim, T. Benavides, D. Gonzalez, T. Akintilo, C. C. Tasan, A. P. Chandrakasan, Y. Fink, P. Anikeeva, Strain-programmable fiber-based artificial muscle. *Science* **365**, 145–150 (2019).

49. Y. Tadesse, N. Thayer, S. Priya, Tailoring the response time of shape memory alloy wires through active cooling and pre-stress. *J. Intell. Mater. Syst. Struct.* **21**, 19–40 (2010).
50. J. Liu, Y. Gao, H. Wang, R. Poling-Skutvik, C. O. Osuji, S. Yang, Shaping and locomotion of soft robots using filament actuators made from liquid crystal elastomer–carbon nanotube composites. *Adv. Intell. Syst.* **2**, 1900163 (2020).
51. A. H. Gelebart, M. Mc Bride, A. P. H. J. Schenning, C. N. Bowman, D. J. Broer, Photoresponsive fiber array: Toward mimicking the collective motion of cilia for transport applications. *Adv. Funct. Mater.* **26**, 5322–5327 (2016).
52. Y. Liu, K. Zhang, J. Ma, G. J. Vancso, Thermoresponsive semi-IPN hydrogel microfibers from continuous fluidic processing with high elasticity and fast actuation. *ACS Appl. Mater. Interfaces* **9**, 901–908 (2017).
53. M. D. Lima, N. Li, M. J. De Andrade, S. Fang, J. Oh, G. M. Spinks, M. E. Kozlov, C. S. Haines, D. Suh, J. Foroughi, S. J. Kim, Y. Chen, T. Ware, M. K. Shin, L. D. Machado, A. F. Fonseca, J. D. W. Madden, W. E. Voit, D. S. Galvão, R. H. Baughman, Electrically, chemically, and photonically powered torsional and tensile actuation of hybrid carbon nanotube yarn muscles. *Science* **338**, 928–932 (2012).

Funding: We acknowledge support from ONR through grant no. N00014-17-1-2062 and the NSF through grant no. CMMI-1554212 and no. CMMI-1762560. **Author contributions:** Q.H., R.C., and S.C. jointly conceived the LCE microfiber and device concepts. Q.H., Zhijian Wang, Y.W., Zijun Wang, C.L., R.A., and J.Z. designed the experiments, fabricated the devices, collected the data, performed the analysis, and interpreted the results. Q.H., R.C., and S.C. wrote the manuscript. All the authors reviews and edited the manuscript. **Competing interests:** The authors declare that they have no competing interests. **Data and materials availability:** All data needed to support the conclusions of this manuscript are included in the main text or Supplementary Materials.

Submitted 12 April 2021
Accepted 29 July 2021
Published 25 August 2021
10.1126/scirobotics.abi9704

Citation: Q. He, Z. Wang, Y. Wang, Z. Wang, C. Li, R. Annapooranan, J. Zeng, R. Chen, S. Cai, Electrospun liquid crystal elastomer microfiber actuator. *Sci. Robot.* **6**, eabi9704 (2021).

Science Robotics

Electrospun liquid crystal elastomer microfiber actuator

Qiguang He, Zhijian Wang, Yang Wang, Zijun Wang, Chenghai Li, Raja Annapooranan, Jian Zeng, Renkun Chen, and Shengqiang Cai

Sci. Robot. **6** (57), eabi9704. DOI: 10.1126/scirobotics.abi9704

Science Robotics (ISSN 2470-9476) is published by the American Association for the Advancement of Science. 1200 New York Avenue NW, Washington, DC 20005. The title *Science Robotics* is a registered trademark of AAAS.